molecular pharmaceutics

pubs.acs.org/molecularpharmaceutics

Article

Influence of Annealing in the Close Vicinity of T_g on the Reorganization within Dimers and Its Impact on the Crystallization Kinetics of Gemfibrozil

Ewa Kamińska,* Aldona Minecka,* Magdalena Tarnacka, Barbara Hachuła, Kamil Kamiński, and Marian Paluch

Cite This: *Mol. Pharmaceutics* 2020, 17, 990−1000

Read Online

ACCESS | Metrics & More | Article Recommendations | Supporting Information

ABSTRACT: In this paper, broadband dielectric spectroscopy (BDS) has been applied to study the molecular dynamics and crystallization kinetics of the antihyperlipidemic active pharmaceutical ingredient (API), gemfibrozil (GEM), as well as its deuterated (dGEM) and methylated (metGEM) derivatives, characterized by different types and strengths of intermolecular interactions. Moreover, calorimetric and infrared measurements have been carried out to characterize the thermal properties of examined samples and to probe a change in the H-bonding pattern in GEM, respectively. We found that the dielectric spectra of all examined compounds, collected below the glass transition temperature (T_g), reveal the presence of two secondary relaxations (β, γ). According to the coupling model (CM) predictions, it was assumed that the slower process (β) is of JG type, whereas the faster one (γ) has an intramolecular origin. Interestingly, the extensive crystallization kinetics measurements performed after applying two paths, i.e., the standard procedure (cooling and subsequently heating up to the appropriate temperature, T_c), as well as annealing at two temperatures in the vicinity of T_g and further heating up to T_c, showed that the annealing increases the crystallization rate in the case of native API, while the thermal history of the sample has no significant impact on the pace of this process in the two derivatives of GEM. Analysis of the dielectric strength ($\Delta\varepsilon$) of the α-process during annealing, together with the results of Fourier transform infrared spectroscopy (FTIR) measurements, suggested that the reorganization within dimeric structures formed between the GEM molecules is responsible for the observed behavior. Importantly, our results differ from those obtained by Tominaka et al. (Tominaka, S.; Kawakami, K.; Fukushima, M.; Miyazaki, A.Physical Stabilization of Pharmaceutical Glasses Based on Hydrogen Bond Reorganization under Sub-T_g Temperature *Mol. Pharm.* **2017** *14* 264 273 10.1021/acs.molpharmaceut.6b00866.), who demonstrated that the sub-T_g annealing of ritonavir (RTV), which is able to form extensive supramolecular hydrogen bonds, protects this active substance against crystallization. Therefore, based on these contradictory reports, one can hypothesize that materials forming H-bonded structures, characterized by varying architecture, may behave differently after annealing in the vicinity of the glass transition temperature.

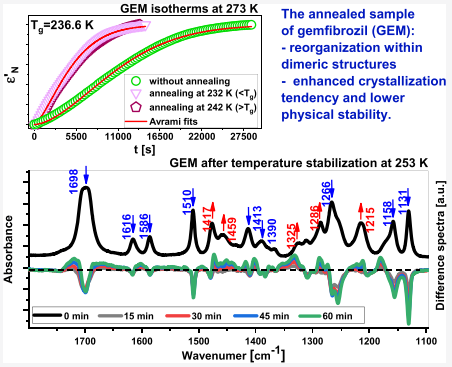

KEYWORDS: *gemfibrozil, chemical modifications, amorphous state, crystallization kinetics, H-bonds, dimeric structures*

INTRODUCTION

In recent years, associated (H-bonded) systems forming supramolecular aggregates, as well as the van der Waals liquids, have been the subject of intensive studies.[1−4] The main aim of these studies is to capture the differences between both types of compounds or to formulate universal patterns/regularities governing their behavior at varying external conditions. The intriguing class of substances are compounds (including numerous active pharmaceutical ingredients (APIs), such as ibuprofen, ketoprofen, indomethacin, and acetaminophen) with a single hydroxyl moiety in the structure. Importantly, these systems, which can create mainly dimeric structures connected by H-bonds (HBs), share the properties of associated substances, as well as the van der Waals liquids.[1] In this context, it should be mentioned that their structural dynamics is strongly sensitive to compression, which is reflected in the high value of the pressure coefficient of the glass transition temperature (dT_g/dp).[1,5−8] Moreover, for these systems, the phenomenological temperature pressure superpositioning rule (TPS), which does not work in the highly associated liquids,[1,9−11] is often satisfied.[6−8]

It is well established that the type of intermolecular interactions in the system not only determines its physical and dynamical properties but also influences the progress of

Received: December 9, 2019
Revised: January 8, 2020
Accepted: January 21, 2020
Published: January 21, 2020

many processes (e.g., crystallization), their mechanisms, and kinetics.[12−14] Therefore, the other problem that is worthy of discussion in the context of the considered classes of materials is the crystallization tendency. In general, in most associated systems, the presence of HBs favors the transition to the glassy state and improves the stability of this phase.[2,12,15] However, this statement is valid mainly for substances that can form extensive H-bonds and create supramolecular structures, such as saccharides (e.g., glucose)[12] or alcohols.[1,16−19] In contrast, the compounds capable of forming dimers/trimers are usually characterized by a lower glass-forming ability (GFA) and simultaneously stronger tendency to crystallization.[12] Such behavior has been shown for many APIs, classified as nonsteroidal anti-inflammatory drugs (NSAIDs), e.g., celecoxib,[20] naproxen,[21,22] flurbiprofen,[23] or acetylsalicylic acid.[24] The impact of dimers on the crystallization rate was also reported for ibuprofen,[7,25] ketoprofen,[8] and indomethacin.[26] However, it should be stressed that according to the classification of amorphous pharmaceuticals proposed by Baird et al.,[27] these three APIs belong to the glasses with low crystallization tendency. The fact that dimeric structures decrease the GFA has also been confirmed in our previous work,[22] where it was demonstrated that the esterification of the carboxylic group of naproxen (NAP) significantly increases its GFA by inhibiting the formation of HBs between the NAP molecules.

Hence, the chemical structure, and thereby the type of intermolecular interactions, is one of the most significant factors determining the glass-forming tendency/physical stability of the given material. This is especially important in the case of amorphous pharmaceuticals (mainly from II and IV groups of the Biopharmaceutical Classification System (BCS)), which are characterized by improved solubility and bioavailability in comparison to their crystalline counterparts. However, the problem with the prediction of their physical stability, due to the change in temperature, humidity, irradiation, and time, seems to be a limiting step toward the better use of these systems in commercial applications.[13,28,29] Therefore, studies on active substances forming dimeric H-bonded structures are crucial not only to better understand their nonintuitive molecular dynamics but also to improve the long-term stability of these amorphous pharmaceuticals. Interestingly, the impact of varying populations of HBs in anti-HIV agent ritonavir (RTV) due to sub-T_g annealing has recently been examined by Tominaka and co-workers.[30] The authors showed that the applied procedure significantly stabilizes this highly associated compound and protects it against crystallization. In this paper, we have selected gemfibrozil (GEM), which was further chemically modified (by replacing the hydrogen from the carboxyl group by the deuterium atom, as well as the methyl moiety) to change the interactions from H-bonded to purely van der Waals ones. It should be mentioned that GEM is an antihyperlipidemic API belonging to the II class of BCS, which is characterized by relatively low GFA, manifested as a strong tendency to crystallization from the amorphous state. In the next step, we performed similar experiments to those carried out by Tominaka et al. to probe the impact of annealing in the vicinity of T_g on the kinetics of the crystallization process in the examined systems.

EXPERIMENTAL SECTION

Materials and Methods. *Materials.* Gemfibrozil, GEM (IUPAC name: 5-(2,5-dimethylphenoxy)-2,2-dimethyl-pentanoic acid, $C_{15}H_{22}O_3$, M_w = 250.33 g/mol), having purity >98% was supplied by TCI Europe and used as received. Deuterated gemfibrozil (dGEM, $C_{15}H_{21}O_3D$, M_w = 251.33 g/mol) and methylated derivative (metGEM, methyl 5-(2,5-dimethylphenoxy)-2,2-dimethyl-pentanoate, $C_{16}H_{24}O_3$, M_w = 264.33 g/mol) have been prepared for the purpose of this paper. dGEM was obtained by the replacement of the hydrogen from the hydroxyl group by deuterium from heavy water, whereas metGEM was synthesized using the esterification procedure of this group. Details of both methods are presented in the Supporting Information (SI). It should be added that GEM and dGEM are white crystalline powders, while metGEM is a clear oily liquid. The chemical structures of investigated compounds are illustrated in Scheme 1.

Scheme 1. Chemical Structure of Gemfibrozil and Its Derivatives

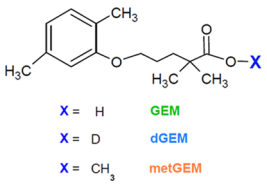

Methods. *Differential Scanning Calorimetry (DSC).* The thermodynamic properties of the examined substances have been investigated using the DSC technique. Calorimetric measurements were carried out using a Mettler Toledo DSC apparatus (Mettler Toledo International, Inc., Greifensee, Switzerland) equipped with a liquid nitrogen cooling accessory and an HSS8 ceramic sensor (heat flux sensor with 120 thermocouples). Temperature and enthalpy calibrations were performed using indium and zinc standards. Each sample was placed in an aluminum crucible (40 μL) and measured at the rate of 10 K/min. The crystalline compounds (GEM, dGEM) were heated inside the DSC apparatus over the melting temperature, next immediately cooled to vitrify the liquid samples, and subsequently scanned to above the respective melting points. In turn, metGEM (a liquid) was cooled to 180 K and then heated to 280 K.

Broad-Band Dielectric Spectroscopy (BDS). Isobaric complex dielectric permittivity measurements ($\varepsilon^*(\omega) = \varepsilon'(\omega) - i\varepsilon''(\omega)$) were taken using the Novocontrol Alpha dielectric spectrometer (Novocontrol Technologies GmbH & Co. KG, Hundsangen, Germany) with the control of temperature provided by a Quatro system, using a nitrogen gas cryostat and stability better than 0.1 K. The data were collected at ambient pressure over the frequency range from 10^{-2} to 10^6 Hz. The sample was placed between two stainless steel electrodes of the capacitor (diameter 10 mm, gap 0.1 mm) and mounted on a cryostat. The molecular dynamics studies were carried out in the following temperature ranges: from 173 K up to 279 K (GEM), from 163 K up to 275 K (dGEM), as well as from 163 K up to 229 K (metGEM) after fast cooling to the glassy state. The crystallization kinetics studies (isothermal measurements) were performed at T = 279, 273, 268, and 265 K (GEM, dGEM), as well as at T = 231, 227, 223, and 219 K (metGEM). The annealing experiments were carried out at temperatures above (T = 242 K for GEM, T = 240 K for dGEM, T = 203 K for metGEM) and below (T = 232 K for GEM, T = 230 K for

https://dx.doi.org/10.1021/acs.molpharmaceut.9b01244
Mol. Pharmaceutics 2020, 17, 990−1000

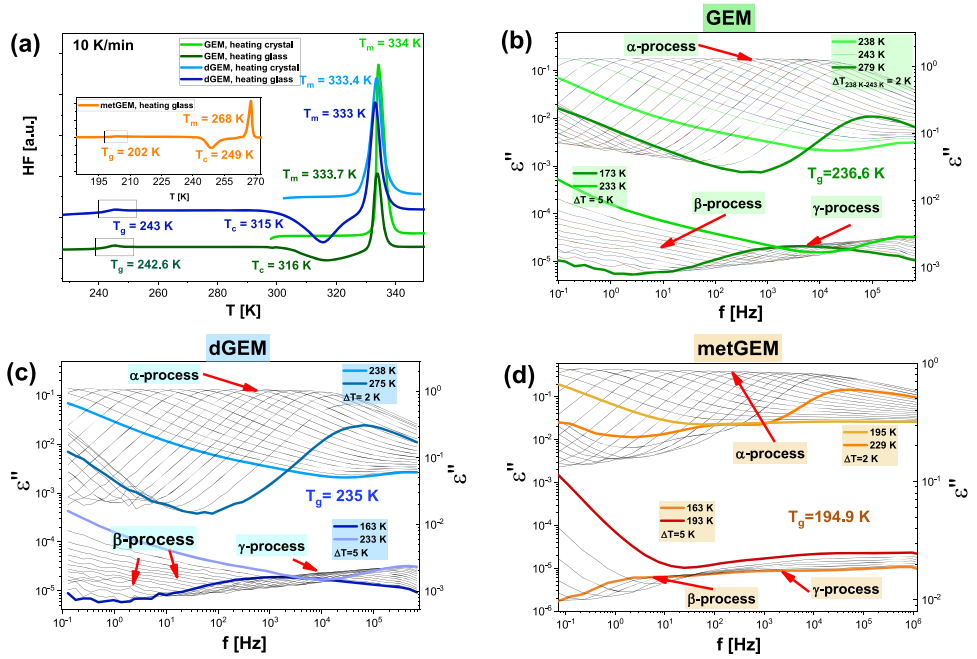

Figure 1. DSC thermograms obtained during heating the crystal and glassy GEM and dGEM with a heating rate of 10 K/min (a). The inset presents a single scan for metGEM, which is a liquid sample. Dielectric loss spectra measured for all studied substances above and below the T_g (b–d).

dGEM, T = 187 K for metGEM) the glass transition points and were continued for about 1 h.

Fourier Transform Infrared Spectroscopy (FTIR). FTIR spectra were measured using the Nicolet iS50 FTIR spectrometer (Thermo Scientific) with a spectral resolution of 4 cm^{-1}. They were recorded in the 4000–800 cm^{-1} frequency range. The bands located below 800 cm^{-1} were not taken into account due to the absorption of CaF_2 windows. The 32 scans were co-added for each spectrum. The glassy/supercooled GEM was obtained by the cooling (30 K/min) of the molten API in a Linkam THMS 600 heating/cooling stage (Linkam Scientific Instruments Ltd., Surrey, U.K.) mounted inside the sample stage of the IR spectrometer. The temperature stabilization accuracy was equal to 0.1 K. The IR spectra were recorded at equal intervals (every 15 min) for 1 h after the temperature stabilization at 253 K. The cell, consisting of the two CaF_2 windows, separated by a 15 μm thick spacer, was used to produce the glassy/supercooled sample of uniform thickness and warrants the constant geometry of the system.

RESULTS AND DISCUSSION

At first, we performed calorimetric measurements to characterize the thermodynamic properties as well as phase transitions in the examined compounds. In Figure 1a, DSC thermograms registered for GEM, dGEM, and metGEM (inset) are presented. In the case of pure API and its deuterated derivative, the crystalline samples were first heated (rate 10 K/min). During this procedure, we observed a single endothermic peak associated with the melting process in both cases. It should be noted that the values of the melting temperature determined for both GEM and dGEM were close to each other (T_m = 334 and 333.4 K, respectively). Moreover, the T_m of neat API stayed in a good agreement with those reported in the literature (332.25–337.4 K).[31−34] Next, the molten samples of GEM and dGEM were cooled to T = 223 K and heated again at the rate of 10 K/min. Upon lowering the temperature, there was no trace of exothermic peaks, suggesting the undergoing crystallization in the examined systems. Moreover, during cooling, as well as the second heating run, a well-visible endothermic event at lower temperatures, assigned to the glass transition phenomenon, was detected in both samples. It is worthwhile to stress that in the case of GEM the temperature of liquid-to-glass transition (T_g = 242.6 K) was comparable to the value determined from the calorimetric studies by Patel and Dave (T_g = 244 K).[33] It should also be mentioned that, analogically to T_ms, the T_gs of GEM and dGEM (243 K) were similar. Besides the glass transition event, an endothermic peak at higher temperatures related to melting, preceded by an exothermic event at $T \sim$ 315 K (indicating the cold crystallization), was noticeable for both samples. Importantly, T_ms obtained during the second heating of GEM and dGEM (333.7 and 333 K) were nearly the same as those of crystal samples (334 and 333.4 K, respectively). This result suggested that both substances recrystallized to the initial polymorphic forms. In turn, in the case of metGEM (a liquid sample at room temperature), only the cooling procedure and the subsequent heating (10 K/min) of the glassy sample were applied (see the inset of Figure 1a). We found that, similarly to GEM and dGEM, three thermal events, one exothermic (related to cold crystallization) and two endothermic (assigned to the glass transition and melting), are noticeable in the collected thermogram. However, the temperatures of these transitions (T_g = 202 K, T_c = 249 K, and T_m = 268 K, respectively) were clearly lower than those of the two previous compounds. Additionally, based on the calorimetric data, we calculated the values of the heat capacity jump at T_g (ΔC_p) for the three examined systems. They were as follows: 0.387 J/g K (GEM), 0.395 J/g K (dGEM), and 0.442 J/g K (metGEM). One can mention that the value of ΔC_p obtained for GEM is close to that reported in the literature for other APIs creating dimeric structures, e.g.,

https://dx.doi.org/10.1021/acs.molpharmaceut.9b01244
Mol. Pharmaceutics 2020, 17, 990−1000

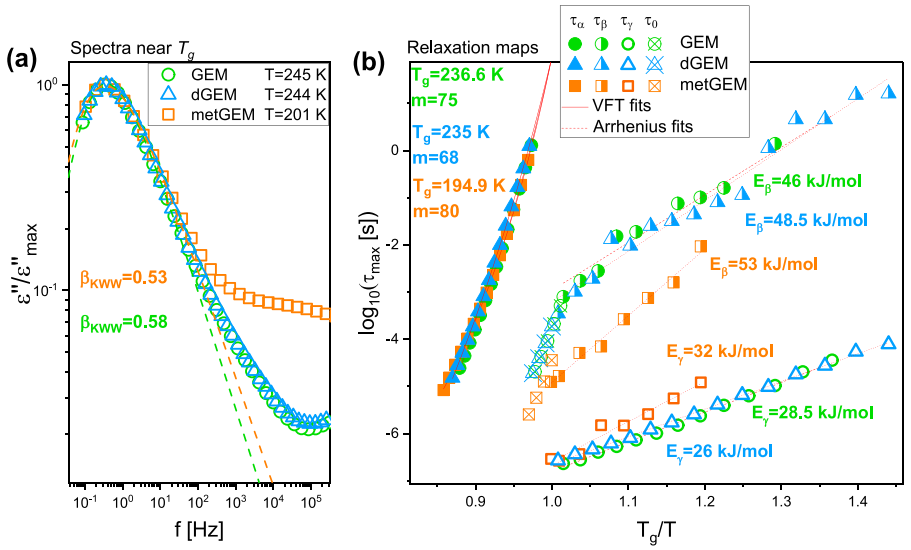

Figure 2. Comparison of the dielectric loss spectra measured at the indicated temperatures near T_g ($f \sim 0.35$ Hz) for GEM, dGEM, and metGEM (a). The spectra were normalized with respect to the maximum dielectric loss (ε''_{max}). The dashed lines are the best KWW fits (eq 6); structural (α) and secondary (β, γ)-relaxation times of native API and its derivatives plotted versus T_g/T (b). The crossed symbols are the primitive relaxation times (τ_0) of the coupling model, calculated for GEM and dGEM with $n = 0.42$ ($\beta_{KWW} = 0.58$), as well as for metGEM with $n = 0.47$ ($\beta_{KWW} = 0.53$), at four different temperatures from the corresponding $\tau\alpha$ given by the VFT fits. The solid and dotted red lines represent the VFT and Arrhenius fits, respectively.

ibuprofen (ΔC_p = 0.362 J/g K)[35] and indomethacin (ΔC_p = 0.417 J/g K).[35] However, it should be noted that for some pharmaceuticals forming H-bonded dimers, e.g., celecoxib and ketoprofen, as well as strongly H-bonded associates, such as ritonavir, the determined values were slightly higher (ΔC_p = 0.440,[36] 0.471,[35] and 0.470 J/g K,[35] respectively) or lower (ΔC_p = 0.298 J/g K[35]—the case of probucol). Moreover, it can be stated that the heat capacity jump at T_g obtained for the deuterated derivative of GEM is practically the same as ΔC_p calculated for neat GEM, despite the weakening of the H-bonds. In turn, the ΔC_p for metGEM (van der Waals system) is somewhat higher than that of GEM and dGEM. Interestingly, the higher value of this thermodynamic parameter in comparison to the neat API was also determined for the methyl, isopropyl hexyl, and benzyl derivative of IBU (thermograms presented in our recent paper):[37] ΔC_p^{IBU} = 0.362 J/g K, while $\Delta C_p^{IBUesters}$ varies within the range 0.487−0.526 J/g K. Based on the above, one can suppose that the change in the intermolecular interactions (from H-bonded to van der Waals) results in the increase in the value of heat capacity jump at T_g for the systems characterized by the very similar backbone.

Having determined the thermal properties of GEM and its two derivatives, we carried out dielectric measurements at ambient pressure and in a wide temperature range. In Figure 1b−d, the dielectric loss spectra collected for GEM, dGEM, and metGEM, above and below the T_g, are presented. As illustrated, in the supercooled liquid phase ($T > T_g$) of all examined compounds, the structural (α) relaxation, followed by dc conductivity connected to the charge transport, can be observed. Both processes move toward lower frequencies (f) with decreasing temperature. Moreover, at higher f, a significant decrease in the amplitude of α-loss peak (indicating the undergoing crystallization) is detected. On the other hand, in the glassy state ($T < T_g$), two secondary relaxation processes (β and γ) with smaller amplitude dominate the spectra of GEM and its two derivatives. The β-process in GEM and dGEM is less visible than the γ one. In the case of metGEM, both secondary relaxations (β, γ) are not well separated from each other and, thus, form one broad peak.

To comprehensively characterize the molecular dynamics of the investigated compounds, the dielectric loss spectra shown in Figure 1b−d were fitted to the one (above the T_g) or superposition of two (below the T_g) Havriliak−Negami (HN) functions with an additional term describing the dc conductivity[38]

$$\varepsilon^*(\bar{\omega}) = \frac{\sigma_{dc}}{\varepsilon_0 \bar{\omega}} + \mathrm{Im} \sum_{j=1}^{2} \left(\varepsilon_\infty + \frac{\Delta\varepsilon_j}{[1 + (i\bar{\omega}\tau_{HN_j})^{\alpha_{HN_j}}]^{\gamma_{HN_j}}} \right) \quad (1)$$

where τ_{HN} is the HN relaxation time, ε_0 is the vacuum permittivity, $\bar{\omega}$ is the angular frequency ($\bar{\omega} = 2\pi f$), $\Delta\varepsilon$ is the dielectric relaxation strength, and α_{HN} and γ_{HN} are the shape parameters, representing the symmetric and asymmetric broadening of the given relaxation peaks, respectively. Next, $\tau_{\alpha,\beta,\gamma}$ were recalculated from τ_{HN} using the formula given in ref 39. The obtained values were plotted as a function of temperatures scaled to T_g in Figure 2b. As can be seen, the relaxation times of the two secondary relaxation processes (β, γ) in metGEM deviate from the respective values determined for the two other compounds. It is especially noticeable in the case of τ_β of methylated derivatives, which are much shorter than those obtained for GEM and dGEM.

To describe the temperature dependencies of τ_α, the Vogel−Fulcher−Tammann (VFT) equation[40−42] was applied (Figure 2b, solid red lines)

$$\tau_\alpha = \tau_{VFT} \exp\left(\frac{D_T T_0}{T - T_0}\right) \quad (2)$$

where τ_{VFT} is the relaxation time at finite temperature, D_T is the strength parameter, and T_0 represents the temperature at which the structural times tend to infinity. Using the VFT fits,

https://dx.doi.org/10.1021/acs.molpharmaceut.9b01244
Mol. Pharmaceutics 2020, 17, 990−1000

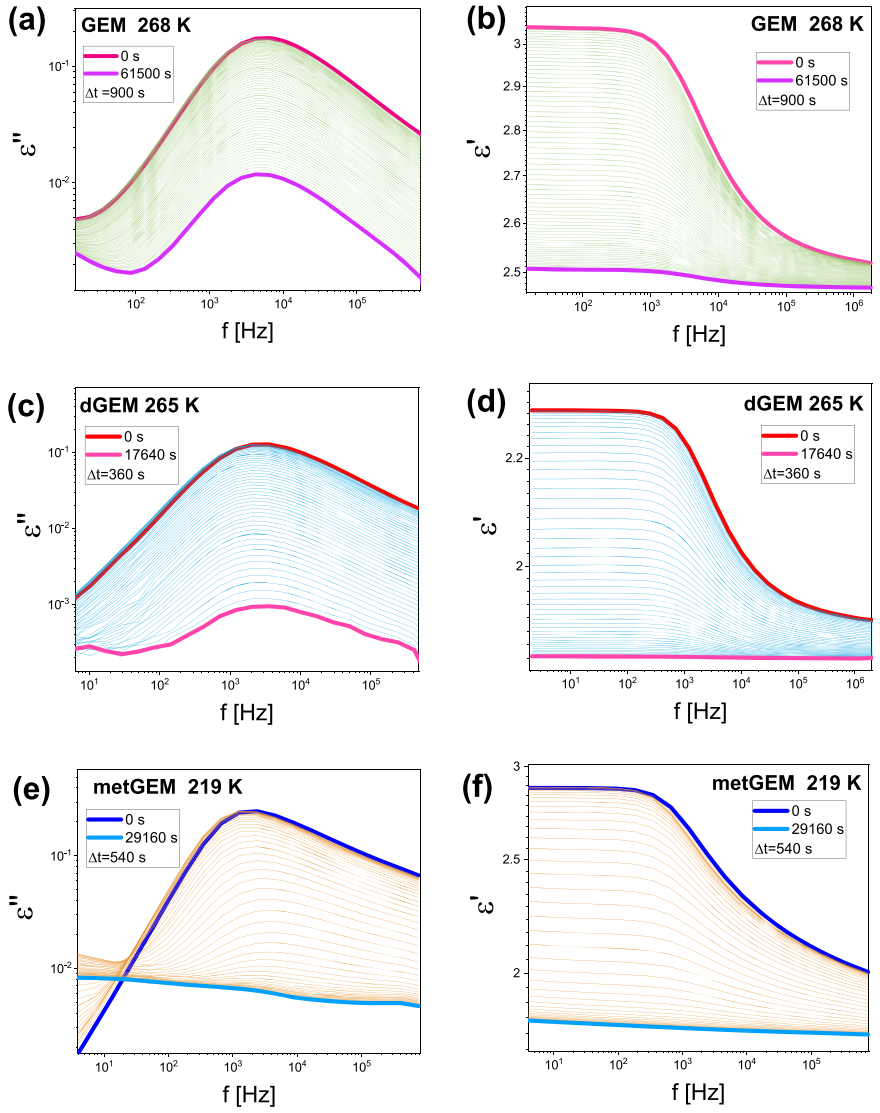

Figure 3. Time evolution of the imaginary (a, c, e) and real (b, d, f) parts of complex dielectric permittivity plotted versus frequency for GEM (a, b), dGEM (c, d), and metGEM (e, f). The isotherms were measured at the indicated temperatures.

the glass transition temperatures (defined herein as temperatures at which τ_α = 100 s) for GEM, dGEM, and metGEM were determined—see Figure 2b. It can be noted that the obtained values are slightly lower than the calorimetric T_gs (see Figure 1a).

Moreover, for three examined compounds, isobaric fragility (m), which describes the sensitivity of the structural process to the temperature changes, was calculated according to the following equation[43]

$$m = \left.\frac{\mathrm{d}\log\tau_\alpha}{\mathrm{d}(T_g/T)}\right|_{T=T_g} \tag{3}$$

Based on the determined values (m = 68−80; Figure 2b), one can classify GEM, dGEM, and metGEM as moderately fragile materials.

In turn, the temperature dependences of secondary (γ and β) relaxation times were fitted to the Arrhenius equation (the red dotted lines in Figure 2b)

$$\tau = \tau_\infty \exp\left(\frac{E_x}{RT}\right), \qquad x = \beta, \gamma \tag{4}$$

where τ_∞ is a pre-exponential factor, R is a gas constant, and E_x is the activation energy. We found that the activation energies of both secondary modes obtained for the van der Waals system, metGEM (E_β = 53 kJ/mol, E_γ = 32 kJ/mol), are slightly higher than those determined for GEM (E_β = 46 kJ/mol, E_γ = 28.5 kJ/mol) and dGEM (E_β = 48.5 kJ/mol, E_γ = 26 kJ/mol), which are capable of forming H-bonded dimeric structures.

To gain a better insight into the molecular origin of the slower (β) and faster (γ) processes observed in the dielectric spectra of the examined compounds, the coupling model (CM) proposed by Ngai[44−46] was applied. It is worth mentioning that this approach is commonly used to distinguish the secondary relaxations having an intermolecular character (called the Johari−Goldstein (JG) type) from those originating from intramolecular motions of some parts of the molecules (the non-JG type). In particular, it links the relaxation time of the given (JG) secondary process (τ_{JG}) and the primitive relaxation time (τ_0) of the CM by the following relation

https://dx.doi.org/10.1021/acs.molpharmaceut.9b01244
Mol. Pharmaceutics 2020, 17, 990−1000

$$\tau_{JG}(T, p) \approx \tau_0(T, p) \quad (5)$$

The value of τ_0 can be determined from the parameters τ_α and β_{KWW} (= 1 − n, where n is a coupling parameter) of the Kohlrausch−Williams−Watts (KWW) function[47,48]

$$\phi_{KWW}(t) = \exp\left[-(\tau/\tau_\alpha)^{\beta_{KWW}}\right] \quad (6)$$

used to fit the α-loss peak at the same temperature, by the CM equation

$$\tau_0 = (t_c)^n(\tau_\alpha)^{1-n} \quad (7)$$

where t_c = 2 ps for small molecular glass-forming liquids. From the analysis of the data (i.e., the normalized dielectric loss spectra of the investigated compounds, measured at selected temperatures close to the T_g) using KWW function (eq 6), the fractional exponent, β_{KWW}, equal to 0.58 (GEM, dGEM) and 0.53 (metGEM—see Figure 2a), which corresponds to n = 0.42 and 0.47, respectively, was obtained. Subsequently, we calculated primitive relaxation times (τ_0) at four temperatures close to the T_g from the corresponding τ_α (VFT fit) of all investigated compounds. As illustrated, the determined values of τ_0 (the crossed symbols in Figure 2b) are very close to the experimental β-relaxation times. Therefore, one can postulate that the slower secondary (β)-relaxation in GEM and its derivatives is a true JG process originating from the local motions of the entire molecules. The faster (γ)-relaxation has the most likely intramolecular character (it is probably related to the rotations of the side alkyl chain in the examined systems).

Besides studying the relaxation dynamics of GEM and its derivatives, we have also performed comprehensive crystallization kinetics studies. Interestingly, we applied two different procedures to measure the progress of this process. The first one was a standard approach—the substances were cooled and next heated to the appropriate crystallization temperatures (T_c). During the second path, the samples were cooled to the two temperatures close to the T_g (one below and one above the T_g), annealed at these T, and finally heated up to the T_c. Dielectric data for all examined samples (the standard procedure) were collected at four T mentioned in the Methods section. In turn, the postannealing isotherms (second approach) were registered at one selected T, in which the first (standard) measurements were also performed. Representative dielectric loss and dispersion spectra obtained during the standard isothermal crystallization of GEM, dGEM, and metGEM are presented in Figure 3a−f, while the analogical data collected before and after annealing at T = 273 K (GEM and dGEM) and T = 223 K (metGEM) are given in the SI (Figures S1−S3). As can be seen, in all cases, the amplitude of the α-relaxation process, as well as the static permittivity, systematically decreases with time, which is a result of freezing out the molecular mobility during crystallization. It should be mentioned that we have compared the dielectric loss spectra measured for three examined compounds before and after annealing at $T \sim T_g$ (see Figure S4 in the SI) and found that there are no differences between them.

To analyze the progress of the crystallization in the examined API and its derivatives (standard and annealing procedures), the measured static permittivity (ε') (Figures 3 and S1−S3) was renormalized using the following equation

$$\varepsilon'_N(t) = \frac{\varepsilon'(0) - \varepsilon'(t)}{\varepsilon'(0) - \varepsilon'(\infty)} \quad (8)$$

where $\varepsilon'(0)$ is the dielectric permittivity at the beginning of the crystallization, $\varepsilon'(\infty)$ is the long-time limiting value, and $\varepsilon'(t)$ is the value at the time, t. In Figure 4a−c, the values of ε'_N have been plotted as a function of time. The data obtained during the standard isothermal crystallization are shown in the main panels, whereas those collected for the samples after annealing are presented in the insets and compared with the ones measured at the same T using the first method. As can be seen, in all cases, the crystallization slows down with decreasing temperature. Moreover, one can notice that for the annealed GEM (the inset of Figure 4a) and dGEM (the inset of Figure 4b) the crystallization proceeds faster, while for metGEM (the inset of Figure 4c) the speed of the process is not affected with respect to the ordinary measurements. To quantify these effects (by determining the constant rates for the crystallization of the investigated samples), the Avrami equation[49,50] was applied

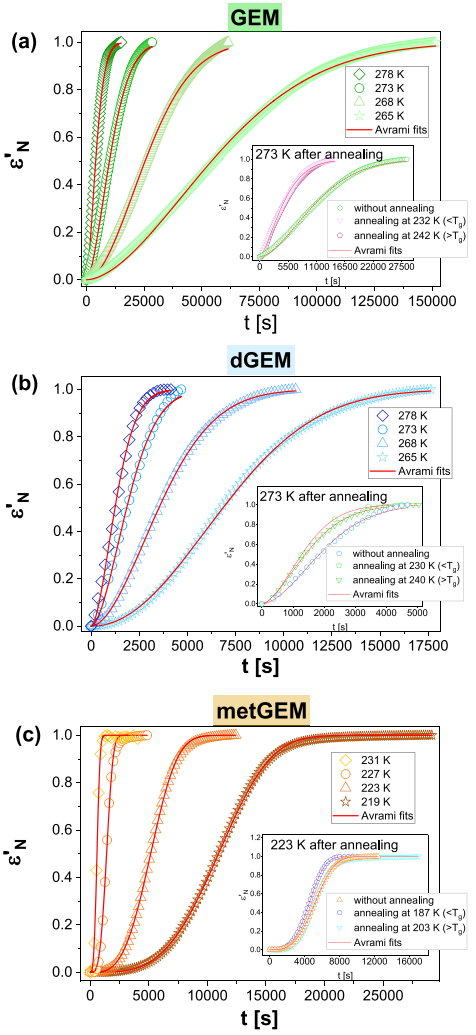

Figure 4. Time dependence of the normalized real permittivity (ε'_N) for GEM (a), dGEM (b), and metGEM (c) obtained during crystallization. The analogous data collected for the samples after the annealing procedure are shown in the insets and compared with those measured for the samples without annealing. The solid red lines represent the Avrami fits in terms of eq 9.

https://dx.doi.org/10.1021/acs.molpharmaceut.9b01244
Mol. Pharmaceutics 2020, 17, 990−1000

$$\varepsilon'_N(t) = 1 - \exp(-kt^{n_{(A)}}) \quad (9)$$

where k is a rate constant, and $n_{(A)}$ is the Avrami exponent, which depends on the crystal morphology.[51] The solid red lines in Figure 4 represent the best fits of eq 9 to experimental data, and, as illustrated, the Avrami model describes them in a satisfactory way. Interestingly, the values of $n_{(A)}$ obtained for GEM, dGEM, and metGEM from the global fitting using eq 9 were as follows: 1.75, 1.93, and 3.48, respectively. This simple comparison indicates the formation of crystals of different morphologies in the methylated derivative of GEM with respect to two other substances. It should also be noted that the Avrami exponents determined from the analysis of the data after annealing of GEM, $n_{(A)}$ = 1.42 (T_{ann} = 242 K) and $n_{(A)}$ = 1.41 (T_{ann} = 232 K), as well as dGEM: $n_{(A)}$ = 1.60 (T_{ann} = 240 K) and $n_{(A)}$ = 1.71 (T_{ann} = 230 K)—see Table S1, were lower than those obtained from fitting the kinetic curves constructed from the standard isothermal measurements. On the other hand, the values of $n_{(A)}$ for metGEM before ($n_{(A)}$ = 3.48) and after annealing ($n_{(A)}$ = 3.60 (T_{ann} = 203 K) and $n_{(A)}$ = 3.57 (T_{ann} = 187 K)) were very close to each other. Based on the above, one can conclude that the annealing does not influence the morphology of the growing crystals in the studied systems.

As a next step, the parameters k obtained from the above-mentioned fitting procedure (standard isothermal data) were plotted versus inverse temperature ($1/T$) in Figure 5. To

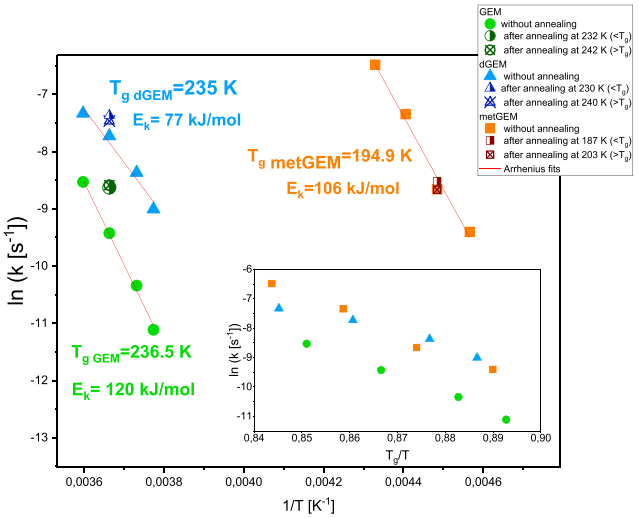

Figure 5. Natural logarithm of the crystallization constant rate, k, for GEM, dGEM, and metGEM plotted versus $1/T$ (main panel), as well as versus T_g/T (inset). The solid red lines denote the fits using eq 10.

estimate the activation barrier for crystallization (E_k) in the examined systems, the dependencies $\ln(k)$ versus $1/T$ were analyzed using the following form of the Arrhenius equation

$$k = k_0 \exp\left(-\frac{E_k}{k_B T}\right) \quad (10)$$

where k_0 is the pre-exponential factor and k_B is a Boltzmann constant. We found that the values of E_k obtained for GEM (E_k = 120 kJ/mol) and metGEM (E_k = 106 kJ/mol) are close to each other, whereas those determined for dGEM are clearly lower (E_k = 77 kJ/mol). Additionally, for all examined samples, we calculated the activation energy of the α-process (E_α) in the temperature range at which the crystallization was carried out. The obtained values were higher than E_k determined for the given compound and changed within the ranges: 161−193, 167−194, and 107−138.0 kJ/mol for GEM, dGEM, and metGEM, respectively. Hence, one can conclude that there is no close relationship between E_α and E_k in the investigated systems. This finding is in line with the data showing the decoupling between the viscosity or reorientational structural dynamics and the rate of the overall crystallization or crystal growth, reported in the literature for several APIs.[52−55]

From Figure 5, one can notice that the crystallization rate of GEM is much lower when compared to those of dGEM and metGEM. It is also evident when we plot ln k versus T_g/T (see the inset of Figure 5). As illustrated, the differences in the speed of crystallization between GEM and other samples (at the same degree of supercooling) are larger than an order of magnitude. Importantly, the data presented in Figure 5 (the crossed symbols) also confirmed that the annealing at T close to T_g affects the progress of crystallization of the nonmodified API in a significant way, while in the other samples the thermal history does not have as much influence on the pace of this process. To explain the obtained results, two possible scenarios can be considered. First, during the isothermal annealing, the nucleation process could have been initiated. Second, the observed behavior might be associated with some equilibration/reorganization in the H-bonding pattern, as has recently been suggested by Tominaka et al.[30] In their paper, the authors showed that the variation in the H-bonding scheme in ritonavir (RTV) due to the sub-T_g annealing inhibits/delays the crystallization. Herein, the situation is much different since crystallization rates of GEM and dGEM increased after the annealing procedure. The discrepancy between the results reported in this work and the one published earlier by Tominaka et al.[30] is probably connected to the fact that RTV has many centers capable of forming extensive HBs, while in the case of GEM there are mainly small dimeric structures. Therefore, due to the annealing, there might be some reorganization in the hydrogen bond pattern or within dimers of API. In this context, it is worth mentioning our previous paper, in which we have explicitly shown that in naproxen (NAP), which also forms dimers, these small structures are responsible for the weak glass-forming ability and the enhanced crystallization of the examined pharmaceutical.

To verify which of the two hypotheses is correct, first we analyzed the representative absorption spectra collected during the annealing of GEM at $T \sim T_g$—see the main panel in Figure 6a. As illustrated, at the time of annealing at T = 242 K, only subtle changes in the position of the structural (α) peak can be detected (the maximum is just slightly shifted toward lower frequencies). By fitting the collected data to the one Havriliak−Negami function (eq 1), we determined the evolution of the dielectric strength ($\Delta\varepsilon$) of the structural process and plotted it as a function of time (t)—see the inset of Figure 6a. As can be seen, the values of $\Delta\varepsilon$ (amplitude of α-peak) slightly increase with time. In this context, it is worthwhile to mention the studies on glycerol carried out by Sanz and Niss.[56] The authors observed that, in contrast to our data, the dielectric permittivity (which is related to the dielectric strength of α-process) decreases with the time during annealing. This effect was related to the nucleation phenomenon. However, it should be stressed that the procedure applied in paper 56 lasted 200 h, whereas GEM and its derivatives were annealed by 1−1.5 h (the short time was used intentionally to avoid the nucleation process—the

https://dx.doi.org/10.1021/acs.molpharmaceut.9b01244
Mol. Pharmaceutics 2020, 17, 990−1000

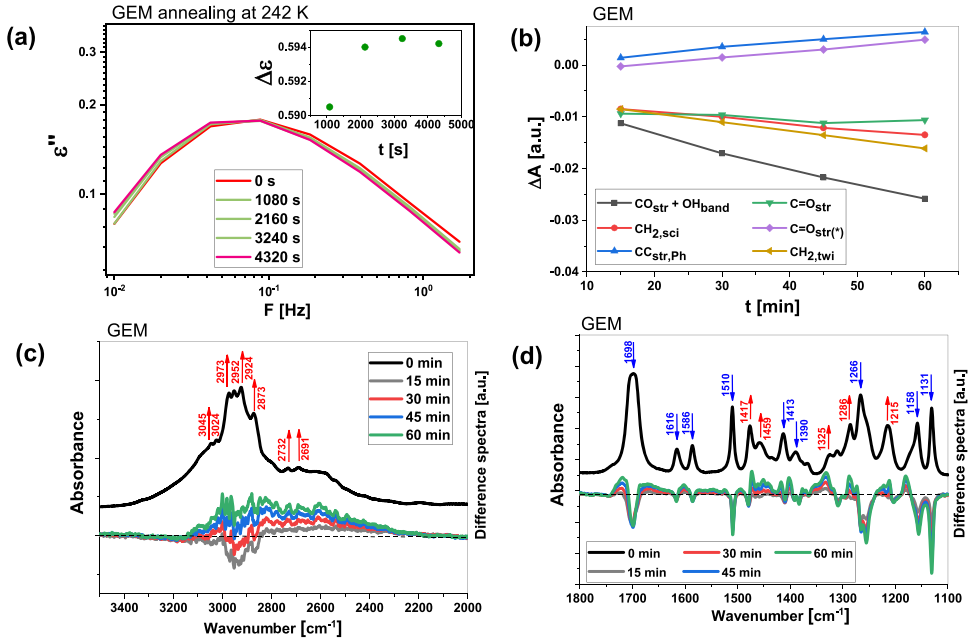

Figure 6. Dielectric loss spectra measured during the annealing procedure at temperatures higher than the T_g for GEM (a). The inset shows the dielectric strength of the structural relaxation plotted as a function of the time of annealing; the kinetic analysis of the absorbance changes for the selected difference bands of GEM (the asterisk symbol in the legend indicates a new component of the C═O stretching vibration band observed at ca. 1720 cm^{-1}) (b); FTIR difference spectra of GEM in the 3500−2000 cm^{-1} (c) and 1800−1100 cm^{-1} (d) frequency ranges, recorded with a 15 min interval and obtained after subtracting the initial spectrum from the time-dependent measurements carried out at 253 K.

degree of crystallinity of our samples after annealing close to T_g was zero). The behavior of the dielectric strength of the α-relaxation for the native GEM shows that the nucleation process, for which rather a decrease in $\Delta\varepsilon$ is expected (as reported by Sanz and Niss), does not occur in the mentioned sample. Moreover, the subtle increase of this parameter with time may suggest some reorganization occurring within the internal structure of GEM.

To probe a possible change in the H-bonding pattern in GEM due to annealing, further FTIR studies were carried out. In panels (c) and (d) of Figure 6, the representative infrared spectra measured at T = 253 K as a function of time, in the two frequency regions, are shown. However, before focusing on the analysis of the time-dependent variation of the FTIR spectra, we will assign the observed experimental bands to the vibrations of the given moieties on the basis of the data published in ref 57. The FTIR spectrum of GEM at T = 253 K is dominated by the presence of a broad, intense band in the region of 3500−2200 cm^{-1}, corresponding to the O−H stretching vibrations, and a very sharp peak at 1698 cm^{-1}, related to the C═O stretching vibration. According to the theoretical results, the bands observed at 3045 and 3024 cm^{-1} are assigned to the C−H stretching vibrations of the aromatic ring of GEM. The asymmetric stretching vibrations of the CH_3 groups attached to the carbon atom of the long chain are detected at 2973 cm^{-1}. In turn, the asymmetric stretching vibrations of the CH_3 groups attached to the benzene ring are located at 2924 cm^{-1}. The peak at 2873 cm^{-1} is ascribed to the symmetric CH_2 stretching vibration, while the one at 1586 cm^{-1} is ascribed to to the ring-breathing vibration. The band at 1477 cm^{-1} originates from the CH_2 scissoring vibration. The medium intense bands at 1413 and 1286 cm^{-1} correspond to the C−C stretching vibrations. The symmetric and asymmetric deformation vibrations of the aliphatic CH_3 groups are observed at 1367 cm^{-1}, whereas the symmetric deformation vibrations of the methyl-substituted benzene derivative appear at 1390 cm^{-1}. The CH_2 twisting vibrations are detected at 1266 cm^{-1}. Finally, the bands at 1215 and 1158 cm^{-1} correspond to the C−H in-plane-bending vibrations.

Having done assignments of the molecular vibrations, we have compared the FTIR spectra measured for the crystalline and supercooled GEM—see Figure S5 in the SI. It was found that the subtle structure and spectral parameters, including the position, full width at half-maximum (FWHM), shape, etc., characterizing the band corresponding to the stretching vibration of the hydroxyl moiety, are very similar in both cases. Therefore, considering the crystallographic data reported for this API in ref 58, one can clearly state that in both crystalline and glassy/supercooled states GEM forms dimers connected via medium-strong H-bonds[59] (the average donor−acceptor distance is in the range of 2.5−3.2 A).

Next, we shifted our attention to the time-dependent FTIR measurements. At first sight the collected spectra (Figure 6c,d) looked the same, and there were no significant variations in the frequencies, widths, and intensities of the absorption bands characteristic of the structure of this substance. However, a closer look indicated that some subtle changes can be detected in several frequency ranges. To illustrate that in a more convincing way, we decided to apply a difference spectra analysis, which relied on the subtraction of the initial FTIR spectrum from the next spectra measured after some time. It was found that the bands visible between 3500 and 2200 cm^{-1} (the O−H stretching), at 1698 cm^{-1} (the C═O stretching), at 1510 cm^{-1} (the CH_2 scissoring deformation), the doublet at 1286 and 1266 cm^{-1} (the aromatic C−C stretching and the CH_2 twisting deformation, respectively), and a band at 1131 cm^{-1} (a mixture vibration of the C−O stretching and O−H bending) exhibit some detectable variations in the intensity that are much above the noise or the spectrometer sensitivity. In fact, they changed in a linear manner with the time of

https://dx.doi.org/10.1021/acs.molpharmaceut.9b01244
Mol. Pharmaceutics 2020, 17, 990−1000

annealing (see Figure 6b). Furthermore, the applied data treatment revealed the complex behavior in the spectral frequency regime connected to the C═O stretching vibration, where a significant negative difference band appears at 1698 cm^{-1}, indicating a loss of absorption in this region (Figure 6d). Simultaneously, a new band component emerges at ca. 1720 cm^{-1}. It is worthwhile to notice that the observed changes within the collected spectra are not due to the variation in the sample size since we have used a 15 μm spacer in the sample holder to warrant the constant sample thickness/geometry during time-dependent measurements. Moreover, the intensity of the absorption peaks did not change monotonically in the whole spectral range over time, since some peaks revealed the increase or decrease in intensity (see Figure 6b). Additionally, the lack of frequency shifts of the selected bands over time indicated that the variation in the FTIR spectra is not related to the undergoing phase transition (nucleation) or conformational change of GEM. It is also worth stressing that, generally, the intensity of the vibrational band is simply proportional to the probability of the transition from the vibrational ground state to the excited state, which in turn depends on the population of the initial state involved in the transition and the change in the dipole moment vector with the vibrational coordinate. Considering these facts, one can hypothesize that the above-described changes in the intensity of the selected bands are most likely related to some reorganization within the dimeric structures of GEM upon annealing at $T \sim T_g$.

This experimental observation, together with the data reported by Tominaka et al.,[30] seems to be very interesting and in some way question the common belief that annealing above the T_g erases the thermal history of the sample. Thus, as far as this procedure is performed in purely the van der Waals liquids (having no tendency to form associates), for which nucleation is avoided, as well as the system geometry and experimental conditions are preserved, it should not make any significant impact on the physical properties or crystallization tendency of these compounds. This hypothesis is somehow confirmed by the data reported herein for metGEM. The situation becomes far more complex in the case of the associating substances. For this particular class of materials, the degree of association and population of more or less complex supramolecular structures, as well as the strength of the H-bonds, may change during the sample annealing in the vicinity of the T_g. Such rearrangements in the H-bonding pattern may have a strong impact on the behavior or crystallization ability of the associating liquids. Furthermore, in the compounds forming self-assemblies of varying architecture and complexity, this effect might be completely different. The above hypothesis is confirmed by the data reported by Tominaka et al.[30] and by us, although, for sure, further thorough studies are required to better understand this quite interesting issue.

CONCLUSIONS

In this paper, the results of the molecular dynamics and crystallization studies (performed using the BDS technique), supported by calorimetric and infrared data for gemfibrozil (GEM) and its two derivatives, deuterated (dGEM) and methylated (metGEM), have been presented. Dielectric measurements showed that besides the dc conductivity and structural (α)-relaxation (observed for all examined compounds at $T > T_g$), two secondary relaxations (β and γ) dominate the loss spectra of glassy samples ($T < T_g$). Analysis using the coupling model (CM) suggested that the slower secondary process, labeled as β, originates from the intermolecular motions of the whole molecules (is a true JG-relaxation), whereas the faster mode (γ) has a rather intramolecular character. The most interesting results were obtained from the crystallization kinetics measurements carried out after applying two procedures: (1) the standard cooling and heating to crystallization temperature (T_c) and (2) the annealing at $T \sim T_g$ just prior to the start of the crystallization process at T_c. These studies showed that the activation barrier of crystallization (E_k) for GEM and metGEM is similar (120 and 106 kJ/mol, respectively), while that determined for dGEM is clearly lower (77 kJ/mol). Moreover, and most importantly, they revealed that the annealing significantly increases the crystallization rate of GEM (H-bonded system), while it has a very weak impact on the pace of this process in the case of dGEM and metGEM (compounds that are characterized by weaker H-bonds and van der Waals interactions, respectively). To explain the observed behavior, we analyzed the changes of the dielectric strength ($\Delta\varepsilon$) of the α-process during the annealing of GEM, as well as the evolution of respective bands (connected to H-bonds) in the infrared spectra. The first analysis excluded the early nucleation as a reason for the enhanced crystallization rate of GEM. In turn, infrared studies suggested that some kind of reorganization within dimers is responsible for this effect. The results obtained herein are in contrast to those published by Tominaka et al.,[30] who suggested that the sub-T_g annealing inhibits the rate of crystallization in H-bonded API ritonavir (RTV), which has many moieties capable of forming extensive HBs. Based on these contradictory reports, one can conclude that the annealing close to the T_g may have a completely different impact on the behavior or crystallization ability in the materials forming H-bonds and supramolecular structures of varying architecture.

ASSOCIATED CONTENT

Supporting Information

The Supporting Information is available free of charge at https://pubs.acs.org/doi/10.1021/acs.molpharmaceut.9b01244.

Description of the determination of dGEM, the procedure of the synthesis of metGEM, crystallization data and comparison of the spectra obtained before and after annealing for all studied substances, as well as the FTIR spectra of crystalline and supercooled GEM (PDF)

AUTHOR INFORMATION

Corresponding Authors

Ewa Kamińska − *Department of Pharmacognosy and Phytochemistry, Faculty of Pharmaceutical Sciences in Sosnowiec, Medical University of Silesia in Katowice, 41-200 Sosnowiec, Poland;* orcid.org/0000-0001-9725-8654; Email: ekaminska@sum.edu.pl

Aldona Minecka − *Department of Pharmacognosy and Phytochemistry, Faculty of Pharmaceutical Sciences in Sosnowiec, Medical University of Silesia in Katowice, 41-200 Sosnowiec, Poland;* orcid.org/0000-0001-5603-032X; Email: aldona.minecka@med.sum.edu.pl

https://dx.doi.org/10.1021/acs.molpharmaceut.9b01244
Mol. Pharmaceutics 2020, 17, 990−1000

Authors

Magdalena Tarnacka − *Institute of Physics and Silesian Center for Education and Interdisciplinary Research, University of Silesia, 41-500 Chorzow, Poland;* orcid.org/0000-0002-9444-3114

Barbara Hachuła − *Institute of Chemistry, University of Silesia, 40-006 Katowice, Poland*

Kamil Kamiński − *Institute of Physics and Silesian Center for Education and Interdisciplinary Research, University of Silesia, 41-500 Chorzow, Poland;* orcid.org/0000-0002-5871-0203

Marian Paluch − *Institute of Physics and Silesian Center for Education and Interdisciplinary Research, University of Silesia, 41-500 Chorzow, Poland*

Complete contact information is available at: https://pubs.acs.org/10.1021/acs.molpharmaceut.9b01244

Notes

The authors declare no competing financial interest.

■ ACKNOWLEDGMENTS

E.K. and A.M. are grateful for the financial support from the National Science Center within the framework of the Sonata BIS project (Grant no. DEC-2016/22/E/NZ7/00266). M.T. and K.K. acknowledge the support received from the National Centre for Research and Development within POIR.04.01.04-00-0142/17.

■ REFERENCES

(1) Floudas, G.; Paluch, M.; Grzybowski, A.; Ngai, K. L. *Molecular Dynamics of Glass-Forming Systems: Effects of Pressure*; Springer-Verlag: Berlin, 2011; Chapter 2.

(2) Wang, R.; Pellerin, C.; Lebel, O. Role of hydrogen bonding in the formation of glasses by small molecules: a triazine case study. *J. Mater. Chem.* **2009**, *19*, 2747−2753.

(3) Roland, C. M.; Bair, S.; Casalini, R. Thermodynamic scaling of the viscosity of van der Waals, H-bonded, and ionic liquids. *J. Chem. Phys.* **2006**, *125*, No. 124508.

(4) Kaminski, K.; Wlodarczyk, P.; Hawelek, L.; Adrjanowicz, K.; Wojnarowska, Z.; Paluch, M.; Kaminska, E. Comparative dielectric studies on two hydrogen-bonded and van der Waals liquids. *Phys. Rev. E* **2011**, *83*, No. 061506.

(5) Atake, T.; Angell, C. A. Pressure Dependence of the Glass Transition Temperature in Molecular Liquids and Plastic Crystals. *J. Phys. Chem. A* **1979**, *83*, 3218−3223.

(6) Wojnarowska, Z.; Adrjanowicz, K.; Wlodarczyk, P.; Kaminska, E.; Kaminski, K.; Grzybowska, K.; Wrzalik, R.; Paluch, M.; Ngai, K. L. Broadband Dielectric Relaxation Study at Ambient and Elevated Pressure of Molecular Dynamics of Pharmaceutical: Indomethacin. *J. Phys. Chem. B* **2009**, *113*, 12536−12545.

(7) Adrjanowicz, K.; Kaminski, K.; Wojnarowska, Z.; Dulski, M.; Hawelek, L.; Pawlus, S.; Paluch, M.; Sawicki, W. Dielectric Relaxation and Crystallization Kinetics of Ibuprofen at Ambient and Elevated Pressure. *J. Phys. Chem. B* **2010**, *114*, 6579−6593.

(8) Adrjanowicz, K.; Kaminski, K.; Tarnacka, M.; Szutkowski, K.; Popenda, L.; Bartkowiak, G.; Paluch, M. The effect of hydrogen bonding propensity and enantiomeric composition on the dynamics of supercooled ketoprofen - dielectric, rheological and NMR studies. *Phys. Chem. Chem. Phys.* **2016**, *18*, 10585−10593.

(9) Casalini, R.; Roland, C. M. Excess wing in the dielectric loss spectra of propylene glycol oligomers at elevated pressure. *Phys. Rev. B* **2004**, *69*, No. 094202.

(10) Paluch, M.; Casalini, S.; Hensel-Bielowka, S.; Roland, C. M. Effect of pressure on the α relaxation in glycerol and xylitol. *J. Chem. Phys.* **2002**, *116*, 9839−9845.

(11) Mierzwa, M.; Paluch, M.; Rzoska, S. J.; Zioło, J. The Liquid−Glass and Liquid−Liquid Transitions of TPP at Elevated Pressure. *J. Phys. Chem. B* **2008**, *112*, 10383−10385.

(12) Kaminski, K.; Adrjanowicz, K.; Wojnarowska, Z.; Dulski, M.; Wrzalik, R.; Paluch, M.; Kaminska, E.; Kasprzycka, A. Do Intermolecular Interactions Control Crystallization Abilities of Glass- Forming Liquids? *J. Phys. Chem. B* **2011**, *115*, 11537−11547.

(13) Rams-Baron, M.; Jachowicz, R.; Boldyreva, E.; Zhou, D.; Jamroz, W.; Paluch, M. *Amorphous Drugs. Benefits and Challenges*; Springer, 2018.

(14) Koperwas, K.; Adrjanowicz, K.; Wojnarowska, Z.; Jedrzejowska, A.; Knapik, J.; Paluch, M. Glass-Forming Tendency of Molecular Liquids and the Strength of the Intermolecular Attractions. *Sci. Rep.* **2016**, *6*, No. 36934.

(15) Laventure, A.; Maris, T.; Pellerin, C.; Lebel, O. Glass versus Crystal: A Balancing Act between Competing Intermolecular Interactions. *Cryst. Growth Des.* **2017**, *17*, 2365−2373.

(16) Pawlus, S.; Klotz, S.; Paluch, M. Effect of Compression on the Relationship between Viscosity and Dielectric Relaxation Time in Hydrogen-Bonded Primary Alcohols. *Phys. Rev. Lett.* **2013**, *110*, No. 173004.

(17) Bauer, S.; Wittkamp, H.; Schildmann, S.; Frey, M.; Hiller, W.; Hecksher, T.; Olsen, N. B.; Gainaru, C.; Böhmer, R. Broadband dynamics in neat 4-methyl-3-heptanol and in mixtures with 2-ethyl-1-hexanol. *J. Chem. Phys.* **2013**, *139*, No. 134503.

(18) Böhmer, R.; Gainaru, C.; Richert, R. Structure and dynamics of monohydroxy alcohols—Milestones towards their microscopic understanding, 100 years after Debye. *Phys. Rep.* **2014**, *545*, 125−195.

(19) Pawlus, S.; Grzybowski, A.; Paluch, M.; Wlodarczyk, P. Role of hydrogen bonds and molecular structure in relaxation dynamics of pentiol isomers. *Phys. Rev. E: Stat., Nonlinear, Soft Matter Phys.* **2012**, *85*, No. 052501.

(20) Grzybowska, K.; Paluch, M.; Wlodarczyk, P.; Grzybowski, A.; Kaminski, K.; Hawelek, L.; et al. Enhancement of Amorphous Celecoxib Stability by Mixing It with Octaacetylmaltose: The Molecular Dynamics Study. *Mol. Pharm.* **2012**, *9*, 894−904.

(21) Balci, K. The effects of conformation and intermolecular hydrogen bonding on the structural and vibrational spectral data of *naproxen* molecule. *Vib. Spectrosc.* **2014**, *70*, 168−186.

(22) Minecka, A.; Kaminska, E.; Tarnacka, M.; Grudzka-Flak, I.; Bartoszek, M.; Wolnica, K.; Dulski, M.; Kaminski, K.; Paluch, M. Impact of Intermolecular Interactions, Dimeric Structures on the Glass Forming Ability of Naproxen, and a Series of Its Derivatives. *Mol. Pharm.* **2018**, *15*, 4764−4776.

(23) Rodrigues, A. C.; Viciosa, M. T.; Danède, F.; Affouard, F.; Correia, N. T. Molecular mobility of amorphous S-flurbiprofen: a dielectric relaxation spectroscopy approach. *Mol. Pharm.* **2014**, *11*, 112−130.

(24) Glaser, R. Aspirin. An ab Initio Quantum-Mechanical Study of Conformational Preferences and of Neighboring Group Interactions. *J. Org. Chem.* **2001**, *66*, 771−779.

(25) Brás, A. R.; Noronha, J. P.; Antunes, A. M.; Cardoso, M. M.; Schönhals, A.; Affouard, F.; Dionísio, M.; Correia, N. T. Molecular Motions in Amorphous Ibuprofen As Studied by Broadband Dielectric Spectroscopy. *J. Phys. Chem. B* **2008**, *112*, 11087−11099.

(26) Taylor, L. S.; Zografi, G. Spectroscopic Characterization of Interactions Between PVP and Indomethacin in Amorphous Molecular Dispersions. *Pharm. Res.* **1997**, *14*, 1691−1698.

(27) Baird, J. A.; Van Eerdenbrugh, B.; Taylor, L. S. A classification system to assess the crystallization tendency of organic molecules from undercooled melts. *J. Pharm. Sci.* **2010**, *99*, 3787−3806.

(28) Wyttenbach, N.; Kuentz, M. Glass-forming ability of compounds in marketed amorphous drug products. *Eur. J. Pharm. Biopharm.* **2017**, *112*, 204−208.

(29) Vasconcelos, T.; Marques, S.; das Neves, J.; Sarmento, B. Amorphous solid dispersions: Rational selection of a manufacturing process. *Adv. Drug Delivery Rev.* **2016**, *100*, 85−101.

(30) Tominaka, S.; Kawakami, K.; Fukushima, M.; Miyazaki, A. Physical Stabilization of Pharmaceutical Glasses Based on Hydrogen

Bond Reorganization under Sub-Tg Temperature. *Mol. Pharm.* **2017**, *14*, 264−273.
(31) Aigner, Z.; Berkesi, O.; Farkasa, G.; Szabó-Révésza, P. DSC, X-ray and FTIR studies of a gemfibrozil/dimethyl-β-cyclodextrin inclusion complex produced by co-grinding. *J. Pharm. Biomed. Anal.* **2012**, *57*, 62−67.
(32) Yang, Q.; Ren, T.; Yang, S.; Li, X.; Chi, Y.; Yang, Y.; Gu, Y.; Hu, C. Synthesis and Pharmacokinetic Study of Three Gemfibrozil Salts: An Exploration of the Structure−Property Relationship. *Cryst. Growth Des.* **2016**, *16*, 6060−6068.
(33) Patel, A. A.; Dave, R. H. Development and Characterization of Innovative Liquid Salt Based Formulations of Sparingly Soluble Drugs. *IJPSR* **2015**, *6*, 2316−2327.
(34) Hussain, T.; Waters, L. J.; Parkes, G. M. B.; Shahzad, Y. Microwave processed solid dispersions for enhanced dissolution of gemfibrozil using non-ordered mesoporous silica. *Colloids Surf., A* **2017**, *520*, 428−435.
(35) Kawakami, K. Ultraslow Cooling for the Stabilization of Pharmaceutical Glasses. *J. Phys. Chem. B* **2019**, *123*, 4996−5003.
(36) Kaushal, A. M.; Bansal, A. K. Thermodynamic behavior of glassy state of structurally related compounds. *Eur. J. Pharm. Biopharm.* **2008**, *69*, 1067−1076.
(37) Minecka, A.; Kaminska, E.; Heczko; Bartoszek, M.; Zięba, A.; Wrzalik, R.; Śmiszek-Lindert, W. E.; Dulski, M.; Kaminski, K.; Paluch, M.; et al. Studying molecular dynamics of the slow, structural, and secondary relaxation processes in series of substituted ibuprofens. *J. Chem. Phys.* **2018**, *148*, No. 224505.
(38) Havriliak, S.; Negami, S. A complex plane analysis of a-dispersions in some polymer systems. *J. Polym. Sci., Part C: Polym. Symp.* **1966**, *14*, 99−117.
(39) Kremer, F.; Schonhals, A. *Broadband Dielectric Spectroscopy*; Springer: Berlin, 2003.
(40) Vogel, H. Das temperaturabhangigkeitgesetz der Viskosität von Flüssigkeiten. *J. Phys. Z* **1921**, *22*, 645−646.
(41) Fulcher, G. S. Analysis of recent measurements of the viscosity of glasses. *J. Am. Ceram. Soc.* **1925**, *8*, 339−355.
(42) Tammann, G.; Hesse, W. Die Abhängigkeit der Viscosität von der Temperatur bie unterkühlten Flüssigkeiten. *Z. Anorg. Allg. Chem.* **1926**, *156*, 245−257.
(43) Angell, C. A. Relaxation in liquids, polymers and plastic crystals—strong/fragile patterns and problems. *J. Non-Cryst. Solids* **1991**, *131*−*133*, 13−31.
(44) Ngai, K. L. An extended coupling model description of the evolution of dynamics with time in supercooled liquids and ionic conductors. *J. Phys.: Condens. Matter* **2003**, *15*, No. S1107.
(45) Ngai, K. L.; Paluch, M. Classification of secondary relaxation in glass-formers based on dynamic properties. *J. Chem. Phys.* **2004**, *120*, 857−873.
(46) Ngai, K. L. *Relaxation and Diffusion in Complex Systems*; Springer, 2011.
(47) Kohlrausch, R. Nachtrag uber die elastiche Nachwirkung beim Cocon und Glasladen. *Ann. Phys.* **1847**, *148*, 353−405.
(48) Williams, G.; Watts, D. C. Non-symmetrical dielectric relaxation behavior arising from a simple empirical decay function. *Trans Faraday Soc.* **1970**, *66*, 80−85.
(49) Avrami, M. Kinetics of phase change. I general theory. *J. Chem. Phys.* **1939**, *7*, 1103−1112.
(50) Avrami, M. Kinetics of Phase Change. II Transformation-Time Relations for Random Distribution of Nuclei. *J. Chem. Phys.* **1940**, *8*, 212−224.
(51) Wunderlich, B. Macromolecular Physics. *Crystal Nucleation, Growth, Annealing*; Academic Press: London, 1976; Vol. 2.
(52) Ediger, M. D.; Harrowell, P.; Yu, L. Crystal growth kinetics exhibit a fragility-dependent decoupling from viscosity. *J. Chem. Phys.* **2008**, *128*, No. 034709.
(53) Bhugra, C.; Shmeis, R.; et al. Prediction of Onset of Crystallization from Experimental Relaxation Times. II. Comparison between Predicted and Experimental Onset Times. *J. Pharm. Sci.* **2008**, *97*, 455−472.
(54) Szklarz, G.; Adrjanowicz, K.; Knapik-Kowalczuk, J.; Jurkiewicz, K.; Paluch, M. Crystallization of supercooled fenofibrate studied at ambient and elevated pressures. *Phys. Chem. Chem. Phys.* **2017**, *19*, 9879−9888.
(55) Mehta, M.; Ragoonanan, V.; McKenna, G. B.; Suryanarayanan, R. Correlation between Molecular Mobility and Physical Stability in Pharmaceutical Glasses. *Mol. Pharm.* **2016**, *13*, 1267−1277.
(56) Sanz, A.; Niss, K. Liquid dynamics in partially crystalline glycerol. *J. Chem. Phys.* **2017**, *146*, No. 044502.
(57) Siva Priya, M.; Asenath Benitta, T.; James, C. Vibrational spectroscopic investigation and normal coordinate analysis of the fibrate hypolipidemic agent 5-(2,5-dimethylphenoxy)-2,2-dimethyl pentanoic acid (Gemfibrozil). *J. Mol. Struct.* **2011**, *990*, 253−262.
(58) Bruni, B.; Coran, S.; Di Vaira, M.; Giannellini, V. 5-(2,5-Dimethylphenoxy)-2,2-dimethylpentanoic acid (gemfibrozil). *Acta Crystallogr., Sect. E: Crystallogr. Commun.* **2005**, *61*, 1989−1991.
(59) Jeffrey, G. A. *An Introduction to Hydrogen Bonding*; Oxford University Press: New York, 1997.

https://dx.doi.org/10.1021/acs.molpharmaceut.9b01244
Mol. Pharmaceutics 2020, 17, 990−1000